Interfacial Phenomena and Heat Transfer, 1 (1): 29–49 (2013)

DETERMINATION OF APPARENT CONTACT ANGLE AND SHAPE OF A STATIC PENDANT DROP ON A PHYSICALLY TEXTURED INCLINED SURFACE

Gaurav Bhutani, K. Muralidhar, & Sameer Khandekar*

Department of Mechanical Engineering, Indian Institute of Technology Kanpur, Kanpur 208016, India

*Address all correspondence to Sameer Khandekar, E-mail: samkhan@iitk.ac.in

Estimating the apparent contact angle under equilibrium conditions is critical for the understanding of several engineering processes. Some examples are dropwise condensation, digital microfluidics, and material deposition schemes. Often, there is considerable uncertainty in the experimental estimation of the contact angle. In this work, we discuss the contact angles and shapes of pendant drops on physically textured inclined surfaces. Two methodologies to determine the apparent contact angles have been employed. In one approach these are obtained from drawing tangents at contact points of micro-droplets in optical images using digital image processing. In the second method, the three-dimensional (3D) Young–Laplace equation is numerically solved using the open-source software, Surface Evolver, by minimizing the sum of the potential and surface energies of the pendant droplet. A section of the numerically obtained 3D droplet shape is then fitted to the experimentally obtained two-dimensional profile using an inverse method. Advancing and receding angles of the imaged drop are calculated by minimizing the error between the numerical and experimental drop shapes, providing good estimates of these angles. In addition, the complete 3D droplet shape is also obtained. The overall methodology presented herein is generic, although the experiments have been conducted with glycerin as the working fluid. The role of surface roughness, plate inclination, and drop volume on the advancing and receding angles of a pendant drop are discussed. On inclined surfaces, the three-phase contact line does not remain pinned and its shape is not circular. The receding angle progressively diminishes with inclination while the advancing angle remains nearly constant.

KEY WORDS: *pendant drop, apparent contact angle, drop profile, advancing and receding angles, Surface Evolver, inverse technique, surface roughness, surface inclination*

1. INTRODUCTION

Surface energy–induced drop movement in microfluidic systems is of importance in microscale thermophysical devices, biological microelectromechanical systems (bio-MEMS), and lab-on-chip applications. Texturing and patterning are physical methods of altering contact angles locally and can be utilized in the design of surface energy gradients. Physical texturing is preferred over chemical techniques because chemical coatings tend to wear off by viscous stresses. In the search for better surfaces, data on contact angles of pendant drops and their sensitivity to substrate inclination and texture are often required. The present study is concerned with developing a formal approach that extracts contact angles from photographic images of drops. Knowledge of the apparent contact angle (referred to as the contact angle in subsequent discussions) and the shape of a pendant drop formed on a substrate are also important in understanding processes such as dropwise condensation, drug delivery, microscale thermophysical engineering, and adhesive technology, to name a few. Equilibrium contact angles, in turn, carry information on surface properties, including wettability and surface energy. An important application requiring detailed knowledge of contact angles as well as the three-dimensional (3D) shapes is the process of vapor condensation as a collection of drops (Sikarwar et al., 2011), particularly of low-conductivity liquids. Dropwise condensation is preferred over the filmwise mode owing to its high heat transfer coefficient and control of the condensation rate, particularly on inclined surfaces (Carey, 1992).

2169–2785/13/$35.00

NOMENCLATURE

B	ratio of excess pressure inside the drop to surface tension at liquid-gas interface (m^{-1})
Bo	Bond number ($= \rho g D^2 \sin\alpha/\gamma$)
D	base diameter of a horizontal drop (m)
D'	base diameter of a drop on an inclined plate (m)
d	maximum drop height in the z direction (m)
g	acceleration due to gravity (m/s^2)
R	radial distance measured from the center of a drop cap (m)
r	root-mean-square roughness of a surface (m)
r'	Wenzel's roughness parameter (= actual surface area/projected surface area)
V_D	volume of the drop (m^3)
z	vertical coordinate taken as positive in the downward direction

Greek Symbols

α	substrate inclination angle (°)
β	polar angle (°)
γ	surface tension (N/m)
Δp	excess pressure inside the drop (Pa)
ζ	coordinate along the symmetry axis in an axisymmetric drop
θ	contact angle (°)
θ_{adv}	advancing angle (°)
θ_E	Young's contact angle (°)
θ_{rec}	receding angle (°)
θ_{min}	minimum contact angle of a three-dimensional drop (°)
θ_{max}	maximum contact angle of a three-dimensional drop (°)
θ_o	horizontal drop contact angle (°)
θ^*	Wenzel's contact angle (°)
κ_m	mean curvature of the liquid–air interface (m^{-1})
μ	liquid viscosity (Pa-s)
ρ_f	density of the liquid (kg/m^3)
σ	axis perpendicular to the symmetry axis in an axisymmetric drop
ϕ	azimuthal angle measured along the three-phase contact line (°)
ψ	angle made by the tangent on the surface of an axisymmetric drop (°)

Here, knowledge of the three-phase contact angle distribution going around the circumference of the condensed liquid droplet is essential to accurately determine the transport rates. Contact angles also govern the interaction of interfacial and body forces acting on sessile and pendant drops. The molecular forces at the three-phase contact line manifest at the macroscopic level as the contact angle and affect steady as well as unsteady transport phenomena.

The physicochemical interaction of liquids on solid surfaces is an active subject of research and has been extensively pursued (Fox and Zisman, 1950; Tuteja et al., 2008; Ajaev et al., 2010; Style and Dyfresne, 2012). Contact angles of various solid–liquid combinations have been reported in the literature. Much of these data are applicable to sessile drops owing to the ease of experimentation. In contrast, pendant drops are difficult to deal with in experiments, especially when the droplet volumes are of the order of microliters. In addition, when the surface on which the pendant drop is deposited is inclined with respect to the horizontal, the advancing angle will be greater than the receding angle. These angles are a function of plate inclination. Overall, the drop is deformed and becomes non-axisymmetric. Although there is an abundance of data on contact angles, there exists a clear gap in the knowledge of contact angles of pendant drops on inclined surfaces. Brown et al. (1980), El Sherbini and Jacobi (2004), and Annapragada et al. (2012) have discussed the effect of plate inclination on the advancing and receding angles of sessile drops. Receding contact angles of sliding drops have also been discussed by Winkels et al. (2011). Cheng et al. (1990) performed experiments on pendant axisymmetric glycerin and water drops to measure the contact angles. On inclined surfaces, the advancing contact angle is different from the receding contact angle and the difference is termed the contact angle hysteresis (CAH).

Factors such as the physical morphology, surface roughness, chemical texture, presence of impurities, nonhomogeneity, anisotropic surface characteristics, substrate inclination, and presence of external body and surface forces affect the equilibrium contact angles of liquid droplets on solid surfaces. Temperature is an important parameter because thermophysical properties depend on it.

One method of altering the wettability of a substrate is to treat it chemically by grafting or adsorbing special promoter molecules with wetting characteristics of their own. This effect of chemical texturing has been previously studied (Wolfram and Faust, 1978; Lee, 1999; Berthier, 2008; Bhushan and Jung, 2011). Chemically textured surfaces have been synthesized to control surface energy gradients and obtain very large contact angles and low CAH (Bico et al., 1999). Such super-hydrophobic surfaces have a contact angle greater than 150° and CAH less than 10°. Furthermore, substrates with designed surface energy gradients can also be formed, which are useful in controlling the flow of drops at low or no plate inclination, and this is an area of extensive research (Chaudhury and Whitesides, 1992; Shastry et al., 2006). In applications where the liquid forming the droplets is highly corrosive—for example, in metal vapor condensation processes—the chemically textured surface usually has a short lifespan. The promoter layer gets leeched away by the condensing liquid droplets, thereby deteriorating the substrate and altering the contact angle. This shortcoming has created a need to alter the surface properties by introducing roughness or through alteration of the physical morphology of the substrate, which can be specifically micro- or nano-patterned or statistically rough (Barthlott and Neinhuis, 1997; Quéré, 2002; Abdelsalam et al., 2005; Bhushan and Jung, 2011). The lotus leaf is a naturally rough surface with a hierarchical physical morphology and has been characterized by many authors, including Barthlott and Neinhuis (1997), Bico et al. (1999), and Bhushan and Jung (2011). Depending on the morphology and the resulting surface energy distribution, a droplet can sit on a solid surface in two distinct configurations. It is said to be in a Wenzel state when it is conformal with the topography, and Wenzel's equation can be used to compute the contact angle (Wenzel, 1936; Berthier, 2008). The other is the Fakir state (Cassie and Baxter, 1944) where the drop only touches the peaks of the physical protrusions present on the surface.

Besides measuring the contact angle at the base of a drop, it is also important to obtain the shape of the three-phase contact line; i.e., the footprint of the drop on the substrate. The contact line is actually in quasi-static equilibrium and its shape changes with the plate inclination (Berejnov and Thorne, 2007). In earlier studies, Wolfram and Faust (1978) and Brown et al. (1980) assumed the contact line was circular for a static drop and pinned everywhere for horizontal and inclined plate configurations. Extrand and Kumagai (1995) measured the aspect ratios of the base contours in water and ethylene glycol drops on polymers. Kalinin et al. (2008) forced the contact line of sessile drops to remain pinned with the inclination by placing them inside photolithographic micro-patterned rings. El Sherbini and Jacobi (2004) showed that the three-phase contact line for a static drop does change with the plate inclination and they fitted the base contour by two ellipses sharing the minor axis. Much of the work reported on the contact line shape involves sessile drops. The present study examines the contact lines of pendant drops on horizontal and inclined surfaces.

Analytical and numerical techniques have been used to predict the drop shapes in two and three dimensions. Brown et al. (1980) used the finite-element method (FEM) to determine the 3D shapes of static drops on inclined plates with an assumption of a circular wetted area. Rio and Neumann (1997) fitted numerical shapes to experimental drop profiles to compute the contact angles and interfacial tensions. The Young–Laplace equation was solved for axisymmetric sessile and pendant drops and the entire drop shape fitted to the experimental measurement. Dingle et al. (2005) used a similar fitting technique to determine the interfacial tension values of axisymmetric drops. Iliev (1995) and Liao et al. (2009) used an iterative method to minimize the overall energy of the system to predict the shapes of sessile drops on horizontal and inclined surfaces. Adamiak (2006) obtained the axisymmetric shape of a conducting liquid drop placed on a hydrophobic dielectric surface with an external electric field. A finite-difference method was used to simultaneously solve the Poisson equation for the electric field and the Young–Laplace equation for the drop shape. The wettability of the system was increased by applying an electric potential difference between the droplet and the counter-electrode. The contact angle was seen to follow the Lippman–Young equation (Mugele and Barrett, 2005; Adamiak, 2006; Berthier, 2008). Pozrikidis (2009) developed a parametric route to numerically solve the Young–Laplace equation and obtained the shapes of axisymmetric sessile and pendant drops. This method has been used to validate the simulations of the present study of a horizontal surface. Santos and White (2011) used the open-source software, *Surface Evolver* (http://www.susqu.edu/brakke/evolver/evolver.html), to simulate the shapes of non-axisymmetric sessile drops. Annapragada et al. (2012) developed a volume-of-fluid (VOF) continuous-surface-force (CSF) model to predict the shapes of sessile droplets under gravity for various substrate inclinations.

In the present study, pendant drops have been imaged for various plate inclinations, substrate roughness, and drop volumes to obtain their equilibrium advancing and receding angles. Glycerin was chosen as the working fluid due to its low vapor pressure and high viscosity. Aluminum and copper surfaces of varying average roughness have been

used as the substrate materials. The apparent contact angles have been estimated using two methods. In Method 1, digital image processing of experimentally obtained images by the tangent method was used. In Method 2, an inverse method was employed that numerically solves the Young–Laplace equation using a variational approach with *Surface Evolver*. Method 2 also yields 3D drop shapes on inclined surfaces. In Method 2, the 3D shape determined numerically is selectively fitted to the experimental drop shape to obtain the contact angles. This approach is similar to that of Rio and Neumann (1997), except that the advancing and receding angles of non-axisymmetric pendant drops obtained by an inverse technique as well as their base shapes are reported in the present study.

2. EXPERIMENTAL APPARATUS AND PROCEDURE

The randomly distributed isotropic roughness of a surface is characterized by its root-mean-square (RMS) value. Three such surfaces with RMS roughness values of around 0.5, 1.5, and 4.0 μm were obtained on aluminum and copper substrates by the wet lapping process. A contact angle measurement goniometric apparatus, developed as part of this work, was used to image the pendant drops on these inclined, randomly textured surfaces. The apparatus [see Fig. 1(a)] can precisely tilt the substrate plate in steps of 1° image the pendant drop from a direction normal to the vertical plane of the tilt; namely, the plane of symmetry of the drop over a range of inclinations (0–45°). Microliter syringes (100 ± 2 and 50 ± 1 μL) were used to deposit liquid pendant drops on the underside of the substrates, with sizes ranging from 5 to 30 μL. The working fluid was glycerin; with density ρ = 1260 kg/m^3, surface tension γ = 63.4 mN/m, and dynamic viscosity μ = 1.069 Pa-s. Glycerin has low volatility and high viscosity, which helps the drop stabilize in a short time period. In addition, results are presented in terms of the Bond number, which enables generalization of the measured data for other liquids. During the experiments, the room temperature was maintained at 20 ± 1°C. A high-resolution progressive scan charge-coupled device camera (Basler A202k: pixel resolution: 1024 × 1024), fitted with a macro-lens, was used to image drops without any wide-angle distortion, with each pixel representing about 6 μm. A dual-channel frame grabber card was used to grab frames from the camera to be stored in a computer hard drive. Post-processing of the droplet images was performed by programs written in *WiT Platform* (Teledyne-Dalsa). *MATLAB* programs extracted the contact angles and drop profiles from the raw images. A pixel-wise scanning algorithm extracted the overall drop profile. The corner pixel was joined to a neighboring pixel to form a tangent. The contact angles have been reported for the eighth neighbor in this study. The angle between this tangent and the horizontal form the basis of the tangent method. To overcome subjectivity in the tangent measurement, an improved inverse technique has been used and is discussed in Sec. 3.2. The drop volume, surface inclination, substrate roughness, and substrate material are the four parameters that were varied in the experiments. Figure 1(b) shows a collection of pendant drop images of a 30 μL glycerin drop on an aluminum surface of 1.46 μm roughness. Changes in the drop shape and contact angles with increasing plate inclination can be clearly seen in Fig. 1(b).

3. NUMERICAL DETERMINATION OF DROPLET SHAPES

The shape of a static drop supported on a solid surface is governed by the Young–Laplace equation, which balances the weight, surface tension, and internal pressure. For two-dimensional (2D) drops, the Young–Laplace equation can be solved using the approach suggested by Pozrikidis (2009). The Young–Laplace equation for 3D axisymmetric drops can be represented using two coordinates, and the solution methodology is presented in Appendix 1. In three dimensions, the equation is rather difficult to solve for non-symmetric cases and alternative approaches are preferred (see Appendix 2). A variational approach was used in the present work to compute the 3D drop shape, wherein the overall energy of the drop (the sum of the potential and interfacial energies) was successively minimized to attain the final equilibrium shape of the static droplet on the substrate. This step was achieved using *Surface Evolver* (Brakke, 1992). Complete information on the 3D shape can be extracted from the minimum energy drop configuration.

3.1 Numerical Solution

This section outlines the numerical method used to obtain the shapes of the pendant drops. To initiate the solution, an imaginary cube of liquid of a given volume is taken and its overall energy is minimized to derive the drop shape under

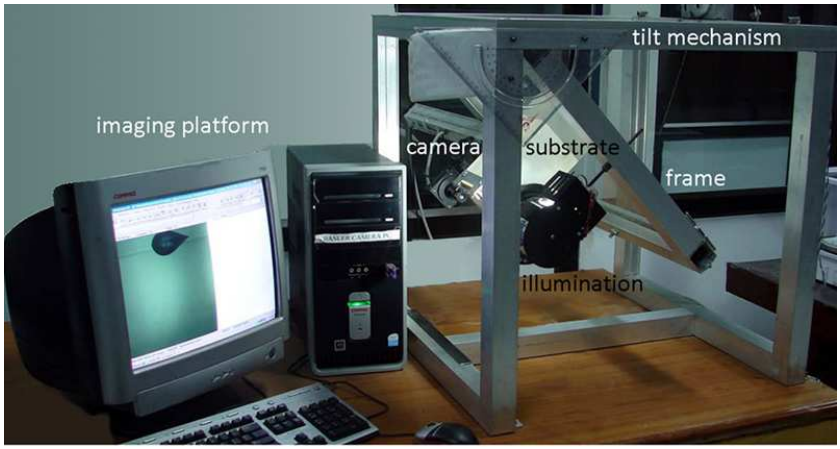

(a)

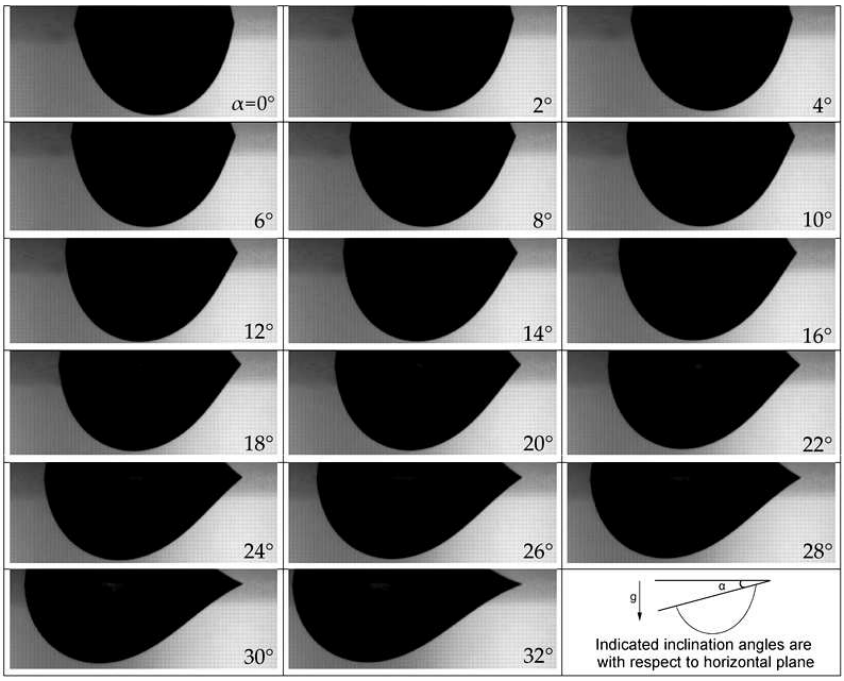

(b)

FIG. 1: (**a**) Photograph of the experimental apparatus and (**b**) images of pendant glycerin drops for various plate inclinations (α): the substrate material is aluminum, plate roughness = 1.46 μm (RMS), and drop volume = 30 μL; the camera turns with the substrate (a slight reflection of the droplet in the metal substrate can be seen at the top of each image; this helps in locating the contact points and measurement of contact angles).

equilibrium conditions. In order to provide the surface energy at the solid–liquid interface, the variation of contact angle as a function of azimuthal angle ϕ needs to be specified. Several studies have been performed in the literature to obtain suitable functions. Functions describing this variation have been suggested by El Sherbini and Jacobi (2004), Dimitrakopoulos and Higdon (1999), Milinazzo and Shinbrot (1988), and Brown et al. (1980). These are shown in Fig. 2(a). El Sherbini and Jacobi (2004) derived the following contact angle variation as a cubic polynomial for sessile drops:

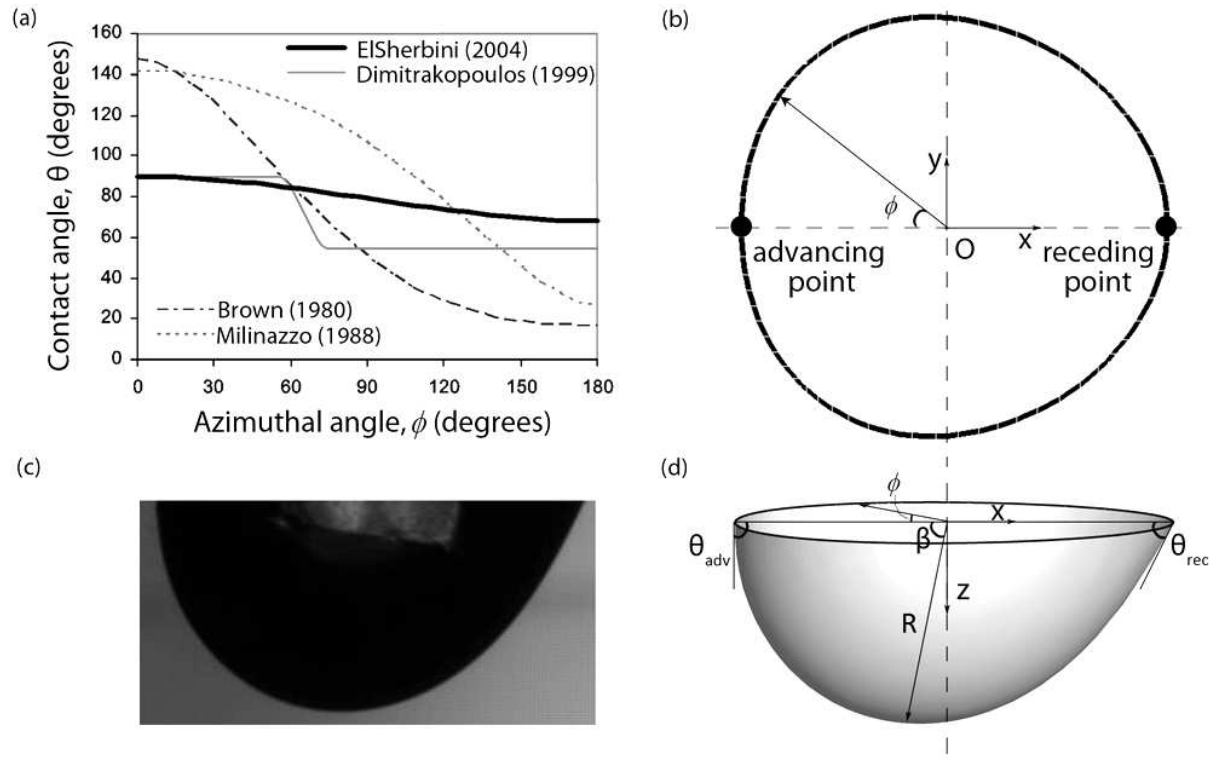

FIG. 2: (**a**) Contact angle as a function of the azimuthal angle as proposed by Brown et al. (1980), Milinazzo and Shinbrot (1988), Dimitrakopoulos and Higdon (1999), and El Sherbini and Jacobi (2004); (**b**) base contour of a 3D drop; (**c**) experimentally recorded image of a pendant drop; and (**d**) numerical simulation of a 3D pendant drop showing the azimuthal angle, which varies from 0 to 360° [advancing angle θ_{adv}, receding angle θ_{rec}, Cartesian coordinates and polar coordinates (angle β and radial distance R)].

$$\theta = 2\frac{\theta_{\max} - \theta_{\min}}{\pi^3}\phi^3 - 3\frac{\theta_{\max} - \theta_{\min}}{\pi^2}\phi^2 + \theta_{\max} \tag{1}$$

Here, $\theta_{\max}$ is the advancing angle, $\theta_{\min}$ is the receding angle, and ϕ is the azimuthal angle, as shown in Fig. 2(b). Liao et al. (2009) assumed the contact angle to vary linearly around the circumference of the drop. Equation (1), also used by Annapragada et al. (2012), was adopted in the present study. The coefficients of the terms of the cubic polynomial in Eq. (1) were obtained using boundary and symmetry conditions.

The algorithmic steps used to obtain the shape of the 3D drop on an inclined surface with the *Surface Evolver* software are the following:

1. Define a cube of liquid with an initial volume equal to the required drop volume V_D.
2. Specify the substrate surface inclination, volume constraint, and physical parameters.
3. Specify the interfacial energy on the solid–liquid contact plane $z = 0$ using the contact angle variation of Eq. (1), with $\theta_{\max}$ and $\theta_{\min}$, as inputs.
4. Specify the gravitational potential energy of the liquid as a function of the plate inclination.
5. Use the gradient descent method in *Surface Evolver* to approach the new 3D drop shape.

6. Correct for the center of the base contour (after each iteration) to calculate azimuthal angle ϕ within *Surface Evolver*.

7. Repeat Steps 3–6 until the drop shape converges to a minimum energy.

The *Surface Evolver* code used to compute pendant drop shapes was first validated for axisymmetric drops against results obtained from the axisymmetric Young–Laplace equation (Appendix 1). Figure 3 compares the shapes of a 30 μL axisymmetric pendant glycerin drop, with a uniform contact angle of 80°, predicted using *Surface Evolver* and the solution of Eqs. (A2) and (A3). The match is seen to be quite good. Figure 4 presents 3D drop images obtained from the numerical simulation of a 30 μL pendant glycerin drop for various plate inclinations. This simulation corresponds to the experimental images shown in Fig. 1(b) for an aluminum substrate of 1.46 μm roughness. The shape of a drop deposited on a rough surface is governed by the same physical equation that balances forces, although the surface roughness alters the contact angle (Bhushan and Jung, 2011). This is realized in the numerical simulation by appropriately setting $\theta_{\min}$ and $\theta_{\max}$ in Eq. (1). The correct values of $\theta_{\min}$ and $\theta_{\max}$ were obtained from the inverse method by comparison against the experiments and the method to obtain these angles is discussed in the next section. Figure 4(a) shows the shapes of the simulated drops from a direction normal to its mid-plane and these are comparable to Fig. 1(b). Figure 4(b) shows an isometric view of these 3D drops for three plate inclinations. A comparison between the experimental and numerical drop shapes can be seen in Fig. 5. The match between the two sets of data is seen to be good.

3.2 Inverse Technique for Estimating Contact Angles

As noted earlier, the contact angles reported in this study have been estimated using two methods: (1) a tangent method for experimental images using digital image processing and (2) an inverse method that minimizes the error between the experimental and numerical drop shapes; the latter being based on assumed contact angles. The inverse method minimizes the error with respect to $\theta_{\max}$ and $\theta_{\min}$ as parameters [Eq. (1)]. An algorithm for calculation of contact angles using the inverse method is presented as follows:

1. Guess $\theta_{\max}$ and $\theta_{\min}$. A good starting guess can be the respective contact angles measured using the tangent method.

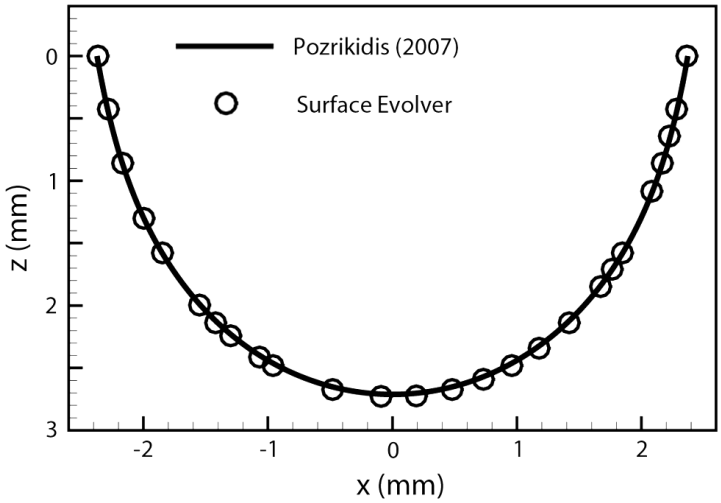

FIG. 3: Validation of the *Surface Evolver* code to predict the shape of a 3D pendant drop; the 3D shape of a 30 μL pendant glycerin drop with a contact angle of 80° is simulated using *Surface Evolver* and is compared with the solution of the axisymmetric Young–Laplace equation on the mid-plane using the parametric form suggested by Pozrikidis (2009).

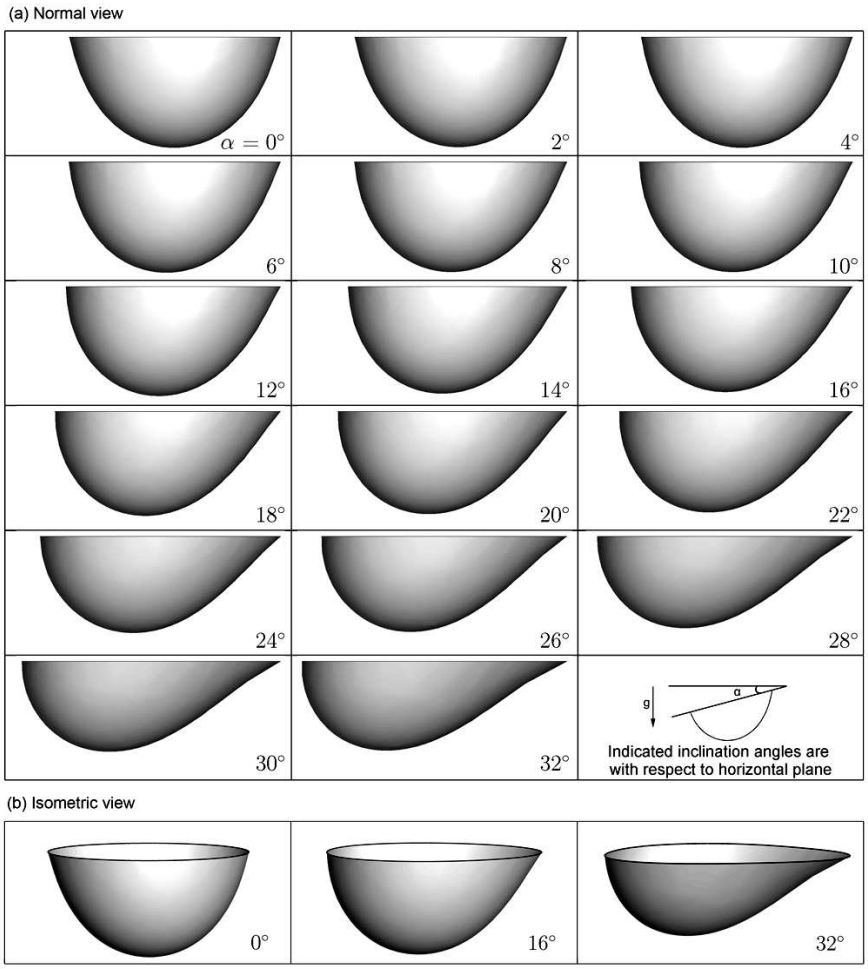

FIG. 4: (**a**) Numerical simulation of a 30 μL pendant glycerin drop on an aluminum substrate of 1.46 μm RMS roughness for various plate inclinations α and (**b**) isometric view of the simulated drops for three plate inclinations.

2. Obtain a 3D drop shape using *Surface Evolver*, as described in Sec. 3.1, for $\theta_{\max}$, $\theta_{\min}$, plate inclination, and fluid properties.
3. Interpolate the 3D triangulated surface and extract the 2D drop curve in the vertical mid-plane.
4. Calculate the RMS error between the 2D numerical and experimental drop shapes. Improve the guessed values of $\theta_{\max}$ and $\theta_{\min}$ using a suitable multivariable optimization method. An exhaustive search method has been used in the present study.
5. Repeat Steps 2–4 to minimize the RMS error obtained in Step 4 with respect to the variables $\theta_{\max}$ and $\theta_{\min}$.
6. The optimum $\theta_{\max}$ and $\theta_{\min}$, corresponding to the minimum RMS error, are reported as the advancing θ_{adv} and receding θ_{rec} angles.

Figure 6 is a contour plot of the error function with respect to $\theta_{\max}$ and $\theta_{\min}$. Error is plotted as a ratio of the RMS error between the experimental and numerical drop profiles and drop diameter D' for the corresponding plate inclination. Drop diameter D' is defined as the maximum drop span along the direction of plate inclination. In Fig. 6,

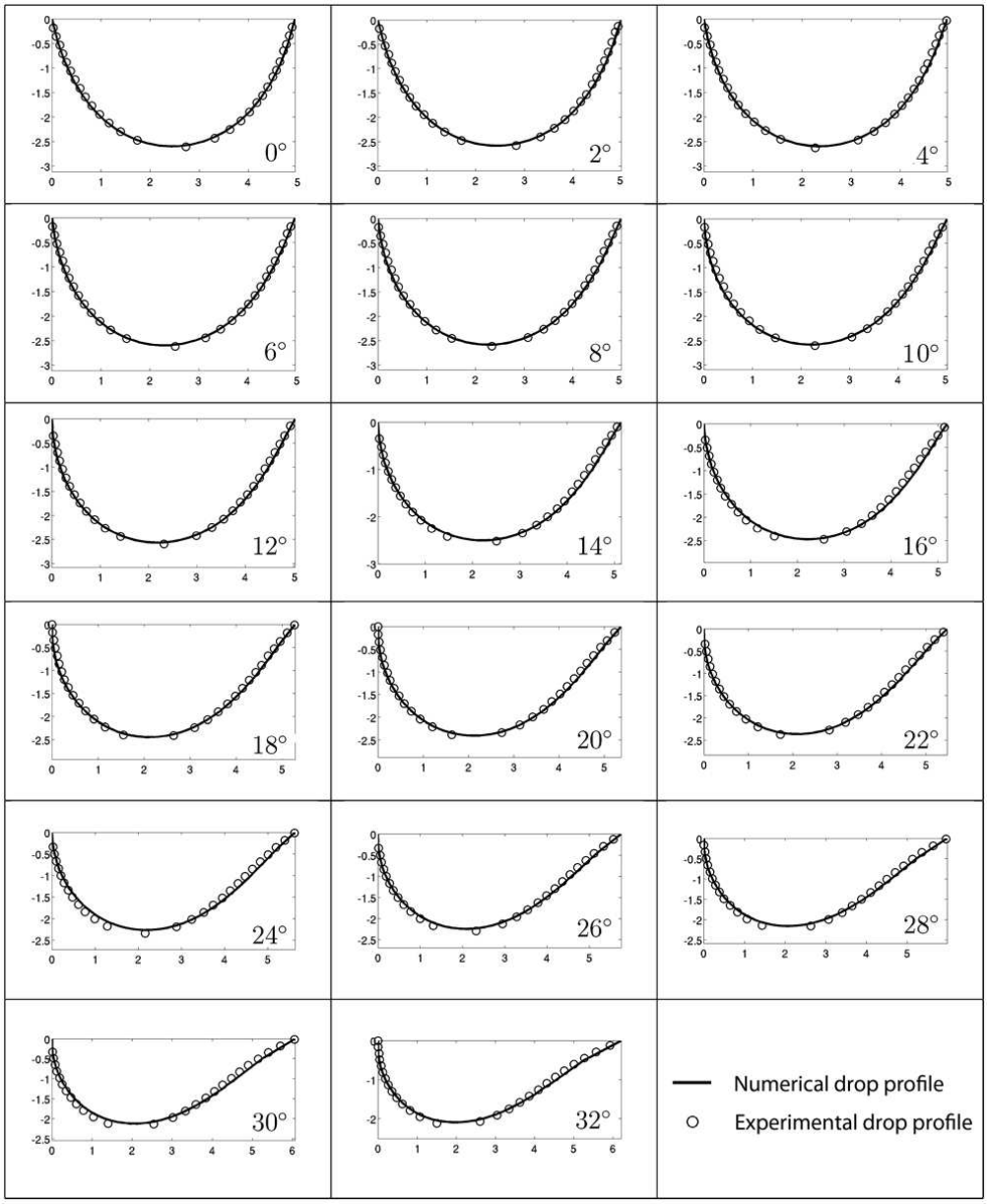

FIG. 5: Comparison of numerical and experimental drop profiles of a 30 μL pendant glycerin drop on an aluminum substrate for various plate inclinations α (RMS roughness = 1.46 μm).

it can be seen that a global minimum exists and forms the basis of the inverse method for measuring the contact angles. This error is most often below 1% and represents an acceptable match between experimental and numerical drop shapes.

A significant level of uncertainty is often involved in the contact angles measured from drop images using the tangent method. The inverse technique overcomes this uncertainty by creating 3D physical drop shapes from a numerical model and fitting 2D sections that are extracted from it to the experimental drop profile. The error associated with the fitting of the entire numerical drop curve to the experimental drop profile is small and has a very small contribution

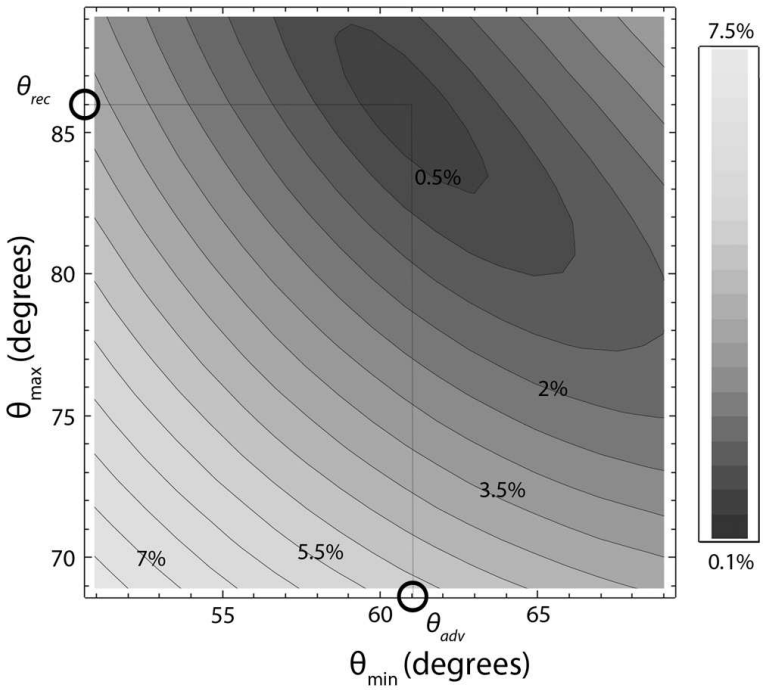

FIG. 6: Contours of error between numerical and experimental profiles for a 15 μL pendant glycerin drop on an aluminum substrate of 1.46 μm RMS roughness inclined at 16° with the horizontal; error has been presented as a ratio of the absolute difference in the drop shapes and its diameter (a clear error minimum is seen; the optimum advancing and receding angles being 86 and 61°, respectively).

from the solid–liquid–vapor interface. Therefore, the inverse contact angles reported in this study are robust for predicting not only the drop shapes but also in providing better estimates of the contact angles compared to the angles estimated from the tangent method.

3.3 Shape of the Three-Phase Contact Line

Besides the knowledge of contact angles, it is important to obtain the shape of the three-phase contact line. The droplet footprint changes with the plate inclination. From the 3D shapes of the non-axisymmetric pendant drops obtained using the variational method, the drop contours can be extracted in the $z = 0$ plane. The base contour starts with a circular shape for a horizontal drop and gets distorted as the substrate plate is inclined. Figure 7 presents the base contours of a 15 μL pendant glycerin drop on an aluminum substrate of 1.45 μm RMS roughness. Unlike the approximations of Wolfram and Faust (1978) and Brown et al. (1980), Fig. 7 shows that the contact line is not pinned everywhere but only at the receding point. With increasing inclination, the liquid mass starts shifting toward the advancing point and the resulting shapes reported in Fig. 7 are obtained. These base contours for inclined pendant drops are qualitatively similar to the experimental images of El Sherbini and Jacobi (2004), although the reference is for a sessile drop. In view of the experimental complexity involved in measuring the three-phase contact line for inclined pendant drops, numerical simulations are seen to offer a convenient alternative.

4. RESULTS AND DISCUSSIONS

Advancing and receding angles have been measured from images of pendant drops of glycerin for a range of plate inclination angles. The effect of volume and surface roughness are considered. Contact angles have been measured

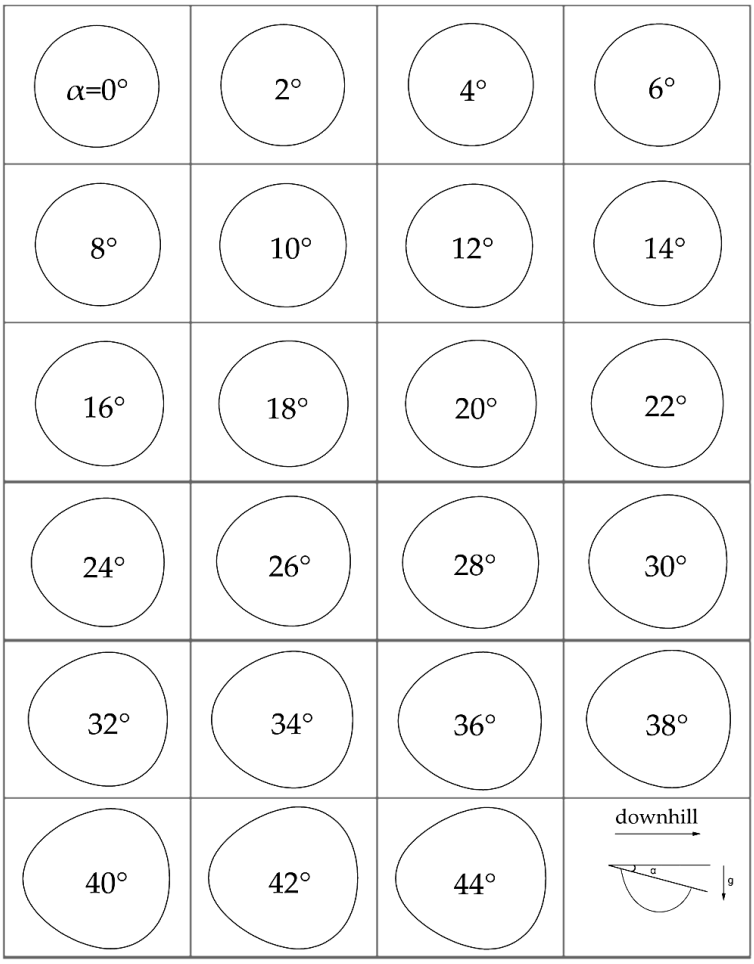

FIG. 7: Numerical simulation of the three-phase contact line for a 15 μL pendant glycerin drop on an aluminum substrate of 1.46 μm RMS roughness as a function of plate inclination α (these contact lines have been extracted from the 3D drop shapes with optimum advancing and receding angles; the diameter of the contact line for the drop over a horizontal surface was 4.1 mm.

using two methods, as noted; i.e. (1) a tangent method where the contact angles are measured from drop images using an image processing technique, and (2) an inverse method that minimizes the error between the experimental and numerical drop shapes. The contact angles corresponding to the minimum error are reported as those measured by the inverse method. Hence, for every experiment, two contact angle values have been reported. The pendant drop was taken to be stationary in this work, and instability and droplet slide-off motion form the scope of future work.

4.1 Physical Texturing

The use of contact angles provides an equivalent representation of the liquid–surface interaction at the three-phase contact line. There are no assumptions on the nature of this contact. At the same time, the force equilibrium relationship is also independent of the nature of the contact. When the proposed inverse method is employed, contact angles that reproduce experimental drop shapes and are consistent with the physical law are predicted as the model parameters.

On surfaces with isotropically distributed roughness, one can expect the Wenzel state to be realized at equilibrium. In general, a drop could be in a Cassie–Baxter state as well. With experimental images as input, the inverse algorithm would recover the contact angles of this configuration as well. In the experiments, it was expected that the drop was in the Wenzel state. This expectation was supported by the modified contact angles seen on the inclined surfaces.

Figures 8 and 9 show the contact angle variations with the surface inclination for pendant glycerin drops of 5 and 30 μL in volume, respectively. In Figs. 8 and 9, the advancing and receding angles are presented for three substrate roughness values; namely, 0.55, 1.46, and 3.98 μm for an aluminum plate. The contact angles plotted in Figs. 8(a) and 9(a) were measured using the tangent method. Figures 8(b) and 9(b) report the contact angles measured using the inverse method. The two sets of data show similar trends. It can be seen that increasing the roughness leads to a reduction in the contact angle. The entire band of advancing and receding angles shifts down by an amount proportional to the roughness, and the band lines remain nearly parallel.

The extent of reduction in the contact angle of the pendant drops with increasing roughness of a horizontal surface can be seen from the three images in Fig. 10(a). Following the Wenzel model (Berthier, 2008)

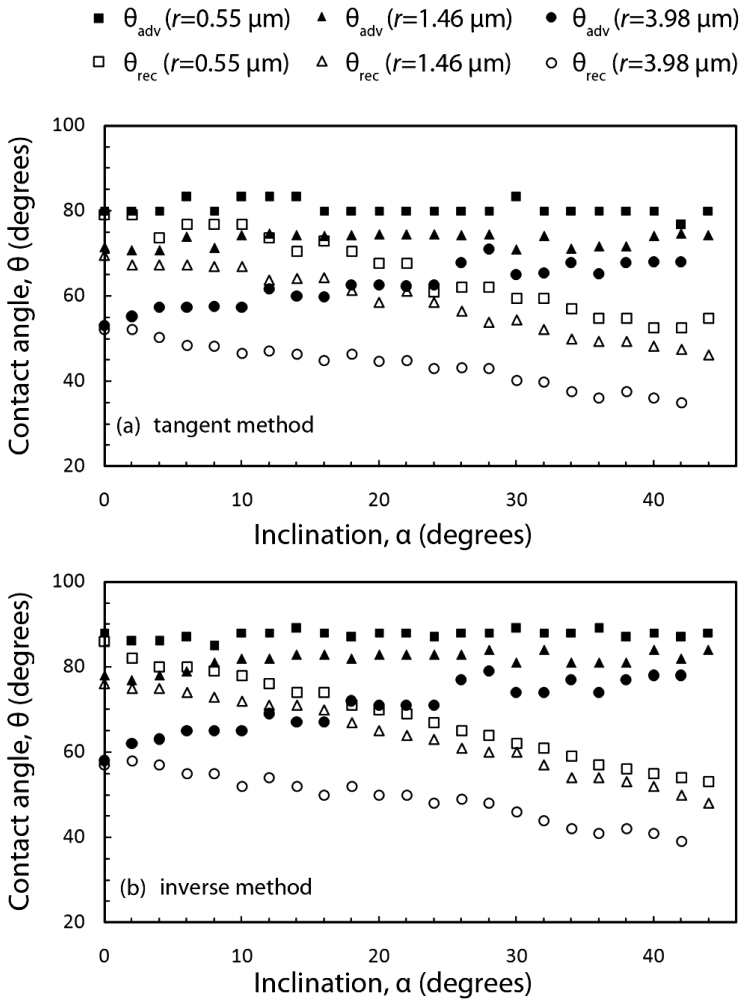

FIG. 8: Contact angle plots of 5 μL pendant glycerin drops on aluminum substrates: advancing and receding angles are plotted against the plate inclination angle for substrate roughness values of 0.55, 1.46, and 3.98 μm (see the legend description at the top); contact angles measured using the tangent method are shown in (**a**) and using the inverse method in (**b**).

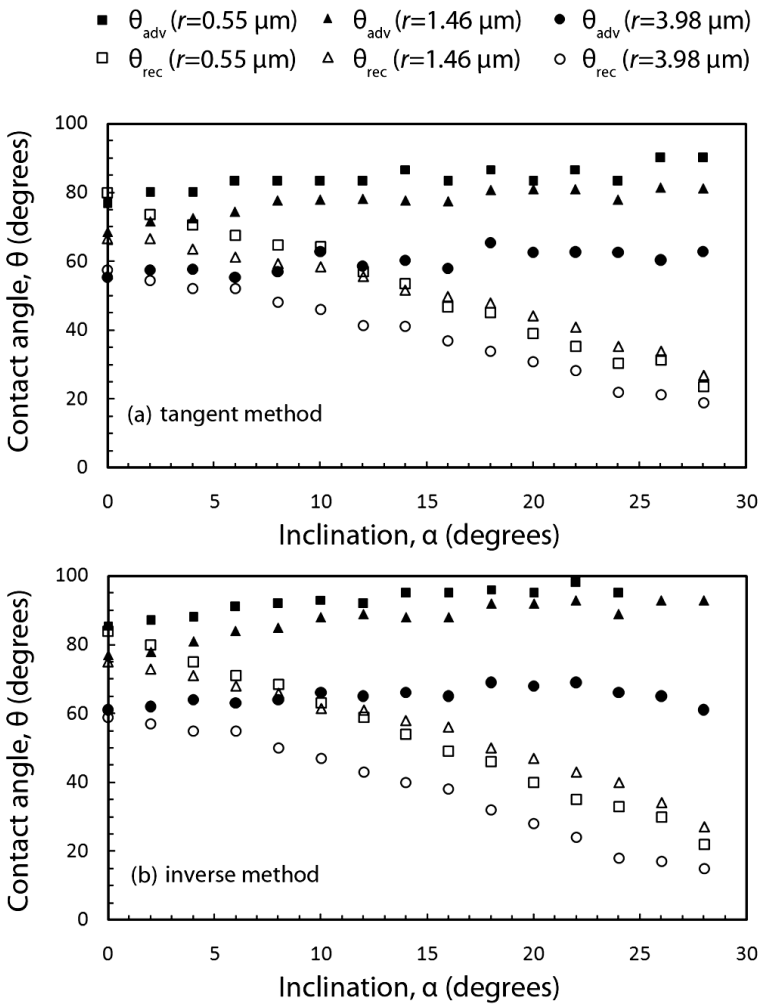

FIG. 9: Contact angle plots of 30 μL pendant glycerin drops on aluminum substrates: advancing and receding angles are plotted against the inclination angle for substrate roughness values of 0.55, 1.46, and 3.98 μm (see the legend description at the top); contact angles measured using the tangent method are shown in (**a**) and using the inverse method in (**b**).

$$\cos\theta^* = r' \cos\theta_E \tag{2}$$

where θ^* is Wenzel's contact angle and θ_E is Young's contact angle. For a horizontal plate, the contact angle for a perfectly smooth aluminum surface in Fig. 10(a) is less than 90° ($\theta_E < 90°$). Wenzel's equation predicts that if roughness $r' > 1$, then $\theta^* < \theta_E$; that is, the contact angle will be less than Young's contact angle. The same effect can be seen for the hydrophilic sessile drops shown in Fig. 10(b). The experimental data presented in Figs. 8 and 9 agree with this theory. On the other hand, for hydrophobic surfaces (i.e., $\theta_E > 90°$), an increase in the surface roughness will lead to an increase in the contact angle [see Fig. 10(b), images iii and iv].

4.2 Plate Inclination

The effect of plate inclination on advancing and receding angles is of major concern in several engineering applications. Figure 11(a) presents the variation of advancing and receding angles with plate inclination for a given surface

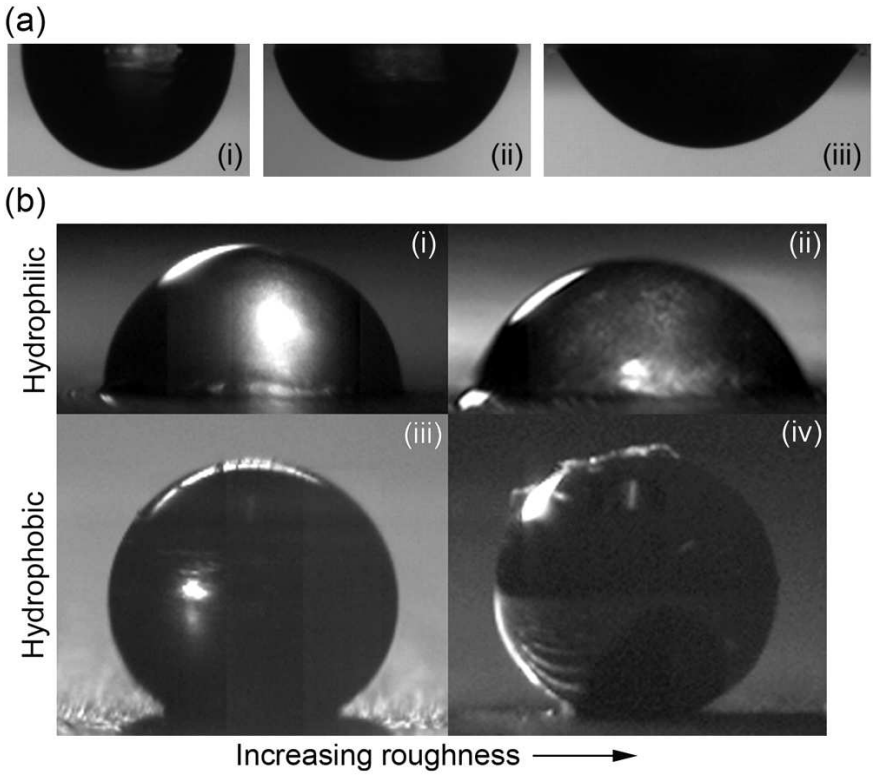

FIG. 10: (**a**) Photographs of 5 μL pendant glycerin drops on aluminum substrates of varying roughness: 0.5 μm (image i), 1.46 μm (image ii), and 3.98 μm (image iii) (the drops show an increase in wettability with increasing surface roughness); (**b**) hydrophilic and hydrophobic sessile drops on surfaces of varying roughness values: 1.4 μm (images i and iii) and 8 μm (images ii and iv) (the contact angle decreases with increase in surface roughness for hydrophilic drops, whereas it increases for hydrophobic drops).

roughness and drop volume. Figure 11(a) shows that inclining the surface causes a monotonic reduction in the receding angle. The advancing angle remains nearly constant for the range of plate inclinations (0–45°) considered in the experiments.

The receding angle normalized with the advancing angle can be considered as a function of the Bond number. Here, the Bond number is given as

$$\mathrm{Bo} = \frac{\rho g D^2 \sin\alpha}{\gamma} \tag{3}$$

with the usual nomenclature. Equation (3) represents the ratio of the component of gravity parallel to the surface that tends to slide the drop and the restoring force of the surface tension. Figure 11(b) shows the variation of $\theta_{\mathrm{rec}}/\theta_{\mathrm{adv}}$ with the Bond number for pendant drops on a textured aluminum surface of 1.46 μm RMS roughness. The functionality has a correlation coefficient of 0.97 for a linear fit, and the regression equation is obtained as

$$\frac{\theta_{\mathrm{rec}}}{\theta_{\mathrm{adv}}} = 1 - 0.303\mathrm{Bo} \tag{4}$$

The above relation is obtained for glycerin drops of volume ranging from 5 to 30 μL on a lapped aluminum substrate of 1.46 μm RMS roughness for plate inclinations between 0 and 45°. Similar empirical expressions were obtained for other surface roughness with an intercept of unity for each. Annapragada et al. (2012) performed a similar analysis for sessile drops and obtained

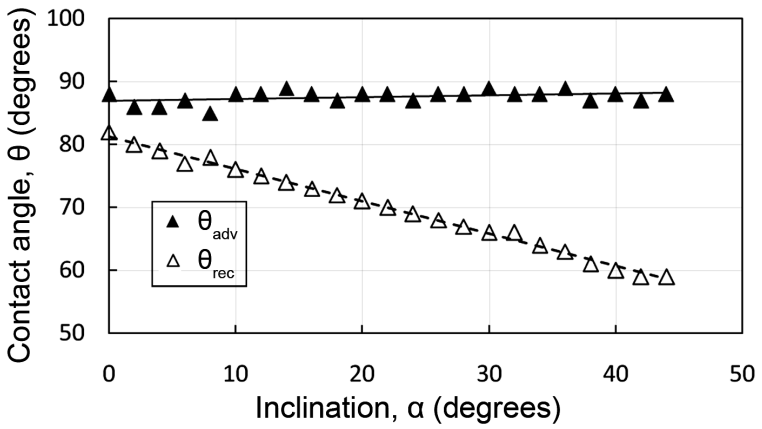

(a)

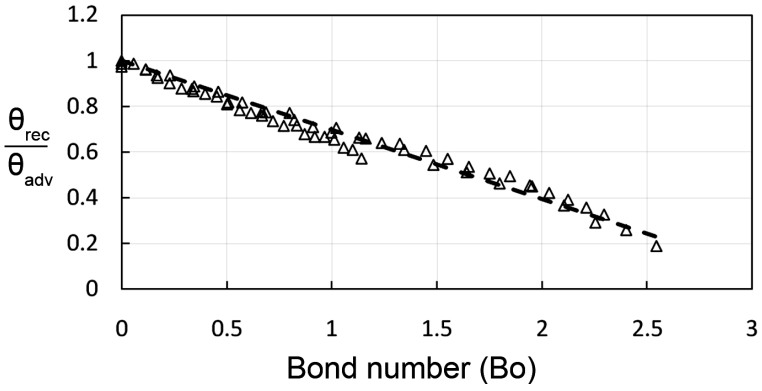

(b)

FIG. 11: (**a**) Advancing and receding angles plotted as a function of plate inclination angle for a 5 μL pendant glycerin drop on a lapped aluminum substrate (0.55 μm RMS roughness; the contact angles measured using the inverse method is reported here); (**b**) $\theta_{\rm rec}/\theta_{\rm adv}$ as a function of the Bond number for glycerin drops of volume ranging from 5 to 30 μL (plate inclination between 0 and 45° on a lapped aluminum surface of roughness 1.46 μm; the contact angles are measured using the inverse method).

$$\frac{\theta_{\rm rec}}{\theta_{\rm adv}} = 1 - 0.298{\rm Bo} \tag{5}$$

The advancing angle in the present study does not change significantly with the plate inclination, and hence

$$\frac{\theta_{\rm adv}}{\theta_o} \approx 1 \tag{6}$$

for the plate inclinations studied. Here, θ_o is the horizontal plate contact angle. Berejnov and Thorne (2007) performed inclination experiments with sessile drops. The advancing angles remained nearly constant with changing plate inclination, whereas the receding angles showed a linear reduction. The present set of results for pendant drops are broadly in agreement with the literature.

At small plate inclinations, the receding point remained pinned, whereas the advancing point started moving. Although the pendant drop was stable, it was in a state of quasi-static equilibrium with its contact line changing continuously with the plate inclination. This phenomenon can be explained by CAH. In the present experiments, pendant drops grew on the substrate from smaller to larger volumes while being deposited using a syringe. Therefore, the horizontal plate contact angles noted here corresponded to their maximum hysteresis values. As the plate was inclined, the

advancing contact angle tried to increase but could not because it had already attained the maximum possible value. The shift in drop mass due to inclination drove the contact line forward at the advancing point, maintaining the advancing angle constant. On the other hand, at the receding point, the contact angle decreased with the inclination. The hysteresis phenomena exhibited by the contact angles allowed this reduction in the receding angle from its extreme value and the receding point remained pinned to the substrate. There is a limit up to which the receding contact angle can decrease as determined by the drop volume, plate inclination, and surface roughness. The drop becomes unstable as soon as the receding contact angle goes below this limiting angle. Instabilities were not captured in our experiments because this study was only concerned with static drops.

Figure 2(b) shows the receding and advancing points on the drop contact line. Figure 12 shows the plot of drop diameter D' with the plate inclination angle for pendant glycerin drops of three volumes; namely, 5, 15, and 30 μL. The variation of drop diameter with plate inclination shows that the contact line is not pinned everywhere. The term drop diameter should be cautiously used because the drop base contour does not remain circular for non-zero plate inclinations. The drop span along the plate inclination is termed the drop diameter. A quadratic polynomial presents a good fit to the drop diameter variation with the plate inclination angle for the range of drop volumes and plate inclinations considered in this study. Figure 7 shows the variation of the shape of the three-phase contact line with the plate inclination.

4.3 Effect of Drop Volume

Figure 13 shows the contact angle plots for the three drop volumes of 5, 15, and 30 μL. As the drop volume increases, the data clearly show that the rate of change of the receding angle with the plate inclination increases. This observation can be interpreted in the following manner: higher volumes show greater sensitivity toward inclination in terms of a change in the receding angle. These results are similar to the sessile drop contact angles obtained by Berejnov and Thorne (2007). In Fig. 13, the horizontal plate contact angles are independent of the drop volume as long as the plate material and roughness are held fixed. The receding-to-advancing angle ratio as a function of the Bond number is shown in Fig. 11(b) and includes the effect of the drop volume. Keeping other factors constant, Fig. 11(b) provides information on the change of the receding contact angle with the drop size.

4.4 Pendant Drops on a Copper Surface

Discussions on the effects of physical texturing, plate inclination, and drop volume on pendant drop contact angles were presented in the previous sections for aluminum surfaces. Copper surfaces were hand lapped similar to aluminum

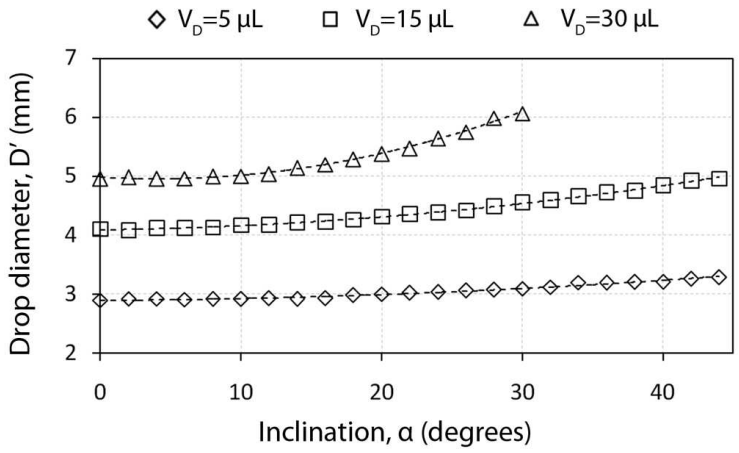

FIG. 12: Variation of pendant drop diameter with plate inclination for three drop volumes (V_D) of 5, 15, and 30 μL: a quadratic polynomial is passed through these data generated with a glycerin drop on an aluminum substrate of 1.46 μm RMS roughness; the drop diameter here is the maximum drop span along the plate inclination direction.

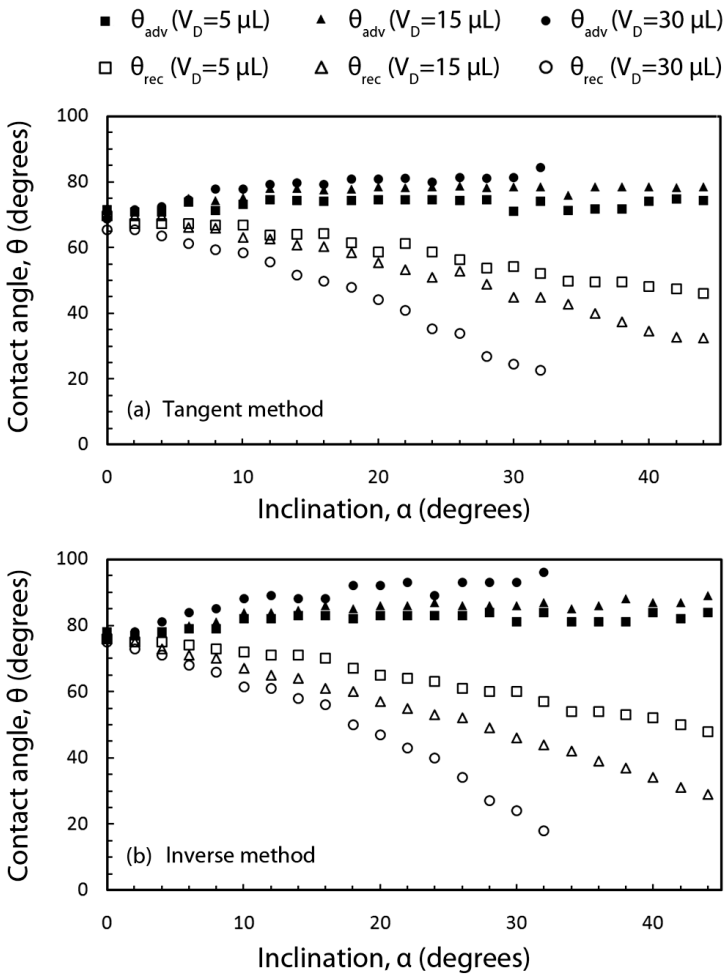

FIG. 13: Contact angle variation of pendant glycerin drops on an aluminum substrate: advancing and receding angles are plotted as a function of the plate inclination for three drop volumes (V_D) of 5, 15, and 30 μL and RMS surface roughness of 1.46 μm; the contact angles plotted in (**a**) are measured using the tangent method whereas (**b**) reports contact angles measured using the inverse method.

to obtain three roughness values; namely, 0.55, 1.46, and 2.7 μm, respectively. The results obtained for the copper surfaces were found to be similar to aluminum, and therefore were not repeated. Figure 14 illustrates the analysis performed on copper for one experimental data point. Figure 14(a) is the experimental image of a 30 μL glycerin drop on a copper substrate of 0.55 μm RMS roughness inclined at 16° with respect to the horizontal. Figure 14(d) is the 3D shape of the drop obtained by solving the mathematical model. Figure 14(b) is the base contour of this deformed drop obtained from the numerical model. Figures 14(c) and 14(e) show the comparison between the experimental and numerical drop shapes in the Cartesian and polar coordinates, respectively. Good agreement between the experimental and numerical drop shapes is clearly visible.

5. CONCLUSIONS

Glycerin drops deposited on the underside of textured aluminum and copper substrates were imaged and analyzed for contact angle data and drop profiles. The experiments were performed by varying the plate inclination, drop volume,

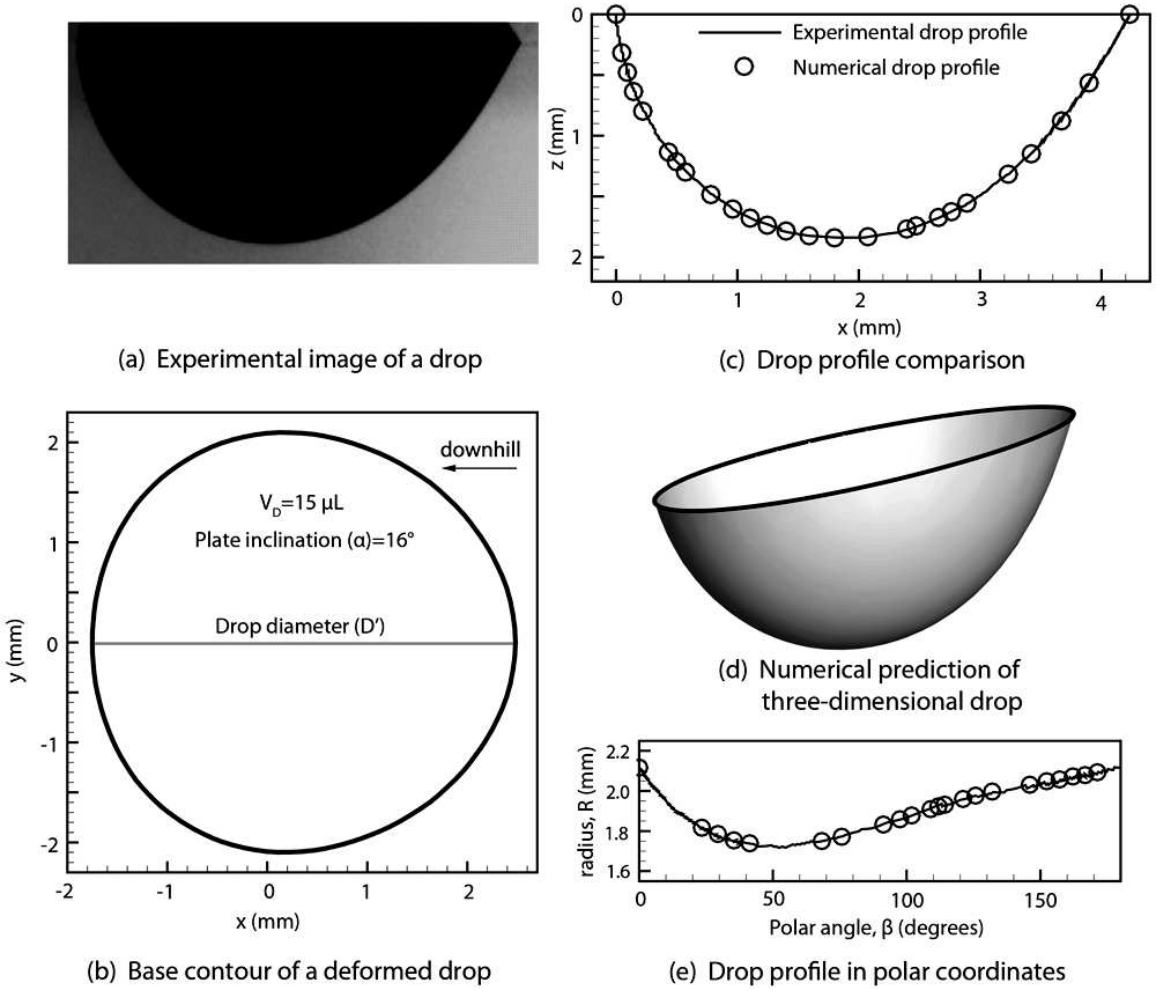

FIG. 14: (**a**) Image of a 30 μL pendant glycerin drop on a copper substrate of 0.55 μm RMS roughness; (**b**) base contour of a deformed drop; (**c**) comparison between experimental and numerical drop profiles in the Cartesian coordinates; (**d**) numerical simulation of the pendant drop considered; and (**e**) polar plot of the drop shape for experimental and numerical drops.

and surface roughness. Advancing and receding angle data as a function of plate inclination were collected on static pendant drops. A numerical model based on open domain software was used to obtain 3D shapes of non-symmetric drops. A novel method to measure the contact angles using an inverse technique was developed in this work. This method measures the contact angles of inclined pendant drops by first solving the 3D variational problem, followed by a comparison of the numerical profiles with the experimental. The error between the experimental and numerical drop shapes was minimized to obtain the best values of the receding and advancing angles. The following results have been obtained in the present work:

1. For static drops, the three-phase contact line of pendant drops has a tendency to move and spread even for small surface inclinations. The advancing point moves gradually, maintaining a nearly constant advancing angle. The receding point remains fixed, allowing the receding angle to decrease linearly with the plate inclination. The movement continues until the drop attains a new equilibrium shape.

2. Increasing surface roughness causes a reduction in the apparent contact angles. The result is in accordance with Wenzel's model, which predicts an increase in wettability for increased surface roughness values for hydrophilic surfaces.

3. The apparent contact angle of a pendant drop on a horizontal surface is not affected by volume. Receding angles fall with a greater slope for larger drop volumes, clearly showing the effect of body forces on deformation.

4. The base contour deforms from a circular shape as the plate is inclined. The numerical model predicts the base contour for inclined pendant drops, providing a convenient alternative to difficult experiments.

REFERENCES

Abdelsalam, M. E., Bartlett, P. N., Kelf, T., and Baumberg, J., Wetting of regularly structured gold surfaces, *Langmuir*, vol. **21**, pp. 1753–1757, 2005.

Adamiak, K., Capillary and electrostatic limitations to the contact angle in electrowetting-on-dielectric, *Microfluid. Nanofluid.*, vol. **2**, pp. 471–480, 2006.

Ajaev, V. S., Gambaryan-Roisman, T., and Stephan, P., Static and dynamic contact angles of evaporating liquids on heated surfaces, *J. Colloid Interface Sci.*, vol. **342**, no. 2 pp. 550–558, 2010.

Annapragada, S. R., Murthy, J. Y., and Garimella, S. V., Droplet retention on an incline, *Int. J. Heat Mass Transfer*, vol. **55**, pp. 1457–1465, 2012.

Barthlott, W. and Neinhuis, C., Purity of the sacred lotus, or escape from contamination in biological surfaces, *Planta*, vol. **202**, pp. 1–8, 1997.

Berejnov, V. and Thorne, R. E., Effect of transient pinning on stability of drops sitting on an inclined plane, *Phys. Rev. E*, vol. **75**, no. 6, p. 066308, 2007.

Berthier, J., *Microdrops and Digital Microfluidics*, 2nd ed., Waltham, MA: Hemisphere, 2008.

Bhushan, B. and Jung, Y. C., Natural and biomimetic artificial surfaces for superhydrophobicity, self-cleaning, low adhesion, and drag reduction, *Prog. Mater. Sci.*, vol. **56**, pp. 1–108, 2011.

Bico, J., Marzolin, C., and Quéré, D., Pearl drops, *Europhys. Lett.*, vol. **47**, no. 2, pp. 220–226, 1999.

Brakke, K., The *Surface Evolver, Exp. Math.*, vol. **1**, no. 2, pp. 141–165, 1992.

Brown, R. A., Orr, F. M., Jr., and Scriven, L. E., Static drop on an inclined plate: Analysis by the finite element method, *J. Colloid Interface Sci.*, vol. **73**, no. 1, pp. 76–87, 1980.

Carey, V. P., *Liquid–Vapor Phase-Change Phenomena*, pp. 342–351, New York: Hemisphere, 1992.

Cassie, A. B. D. and Baxter, S., Wettability of porous surfaces, *Trans. Faraday Soc.*, vol. **40**, pp. 546–551, 1944.

Chaudhury, M. K. and Whitesides, G. M., How to make water run uphill, *Science*, vol. **256**, no. 5063, pp. 1539–1541, 1992.

Cheng, P., Li, D., Boruvka, L., Rotenberg, Y., and Neumann, A. W., Automation of axisymmetric drop shape analysis for measurements of interfacial tensions and contact angles, *Colloids Surf.*, vol. **43**, pp. 151–167, 1990.

Dimitrakopoulos, P. and Higdon, J. J. L., On the gravitational displacement of three-dimensional fluid droplets from inclined solid surfaces, *J. Fluid Mech.*, vol. **395**, pp. 181–209, 1999.

Dingle, N. M., Tjiptowidjojo, K., Basaran, O. A., and Harris, M. T., A finite element based algorithm for determining interfacial tension from pendant drop profiles, *J. Colloid Interface Sci.*, vol. **286**, no. 2, pp. 647–660, 2005.

El Sherbini, A. I. and Jacobi, A. M., Liquid drops on vertical and inclined surfaces: I. An experimental study of drop geometry, *J. Colloid Interface Sci.*, vol. **273**, no. 2, pp. 556–565, 2004.

Extrand, C. W. and Kumagai, Y., Liquid drops on an inclined plane: The relation between contact angles, drop shape, and retentive force, *J. Colloid Interface Sci.*, vol. **170**, no. 2, pp. 515–521, 1995.

Fox, H. W. and Zisman, W. A., The spreading of liquids on low energy surfaces. I. polytetrafluoroethylene, *J. Colloid Sci.*, vol. **5**, no. 6, pp. 514–531, 1950.

Iliev, S. D., Iterative method for the shape of static drops, *Comput. Methods Appl. Mech. Eng.*, vol. **126**, no. 3, pp. 251–265, 1995.

Kalinin, Y., Berejnov, V., and Thorne, R. E., Controlling microdrop shape and position for biotechnology using micropatterned rings, *Microfluid. Nanofluid.*, vol. **5**, pp. 449–454, 2008.

Lee, Y. L., The wettability of solid surfaces modified by vacuum deposition of stearic acid, *Colloid Surf., A*, vol. **155**, nos. 2–3, pp. 221–229, 1999.

Liao, Q., Shi, Y., Fan, Y., Zhu, X., and Wang, H., Numerical simulations of the equilibrium shape of liquid droplets on gradient surfaces, *Appl. Therm. Eng.*, vol. **29**, no. 2, pp. 372–379, 2009.

Milinazzo, F. and Shinbrot, M., A numerical study of a drop on a vertical wall, *J. Colloid Interface Sci.*, vol. **121**, no. 1, pp. 254–264, 1988.

Mugele, F. and Baret, J. C., Electrowetting: From basics to applications, *J. Phys.: Condens. Matter*, vol. **17**, pp. R705–R774, 2005.

Pozrikidis, C., *Fluid Dynamics: Theory, Computation, and Numerical Simulation*, 2nd ed., New York: Springer, 2009.

Quéré, D., Rough ideas on wetting, *Physica A*, vol. **313**, nos. 1–2, pp. 32–46, 2002.

Rio, O. D. and Neumann, A. W., Axisymmetric drop shape analysis: Computational methods for the measurement of interfacial properties from the shape and dimensions of pendant and sessile drops, *J. Colloid Interface Sci.*, vol. **196**, no. 2, pp. 136–147, 1997.

Santos, M. J. and White, J. A., Theory and simulation of angular hysteresis on planar surfaces, *Langmuir*, vol. **27**, no. 24, pp. 14868–14875, 2011.

Shastry, A., Case, M. J., and Böhringer, K. F., Directing droplets using microstructured surfaces, *Langmuir*, vol. **22**, no. 14, pp. 6161–6167, 2006.

Sikarwar, B. S., Battoo, N. K., Khandekar, S., and Muralidhar, K., Dropwise condensation underneath chemically textured surfaces: Simulation and experiments, *ASME J Heat Transfer*, vol. **133**, no. 2, p. 021501, 2011.

Style, R. W. and Dufresne, E. R., Static wetting on deformable substrates, from liquids to soft solids, *Soft Matter*, vol. **8**, pp. 7177–7184, 2012.

Tuteja, A., Choi, W., McKinley, G. H., Cohen, R. E., and Rubner, M. F., Design parameters for superhydrophobicity and superoleophobicity, *MRS Bull.*, vol. **33**, pp. 752–758, 2008.

Wenzel, R. N., Resistance of solid surfaces to wetting by water, *Ind. Eng. Chem.*, vol. **28**, pp. 988–994, 1936.

Winkels, K. G., Peters, I. R., Evangelista, F., Riepen, M., Daerr, A., Limat, L., and Snoeijer, J. H., Receding contact lines: From sliding drops to immersion lithography, *Eur. Phys. J. Spec. Top.*, vol. **192**, no. 1, pp. 195–205, 2011.

Wolfram, E. and Faust, R., *Wetting, Spreading and Adhesion*, J. F. Padday, ed., pp. 213–222, London: Academic, 1978.

APPENDIX 1: PARAMETRIC FORM OF THE AXISYMMETRIC YOUNG–LAPLACE EQUATION

The Young–Laplace equation represents the force equilibrium for a static drop and takes the following form for an axisymmetric pendant drop (Pozrikidis, 2009):

$$2\kappa_m = \frac{\zeta}{l^2} + B \tag{A1}$$

Here, ζ is the symmetry axis; σ is the other axis perpendicular to ζ and $\sigma = f(\zeta)$ with the origin at the lowest point of the pendant drop; κ_m is the mean curvature given by $\kappa_m = (\kappa_1 + \kappa_2)/2$, where $\kappa_1 = -f''/(1 + f'^2)^{3/2}$ and $\kappa_2 = 1/f(1 + f'^2)^{1/2}$; $l = \sqrt{\gamma/\Delta\rho g}$ is the capillary length. One can introduce a parameter ψ, the angle made by the tangent on the drop at any point on its surface in Eq. (A1), to convert it into the following set of ordinary differential equations:

$$\frac{d\zeta}{d\psi} = \frac{\sin\psi}{Q} \tag{A2}$$

$$\frac{d\sigma}{d\psi} = -\frac{\cos\psi}{Q} \tag{A3}$$

Here, $Q = (\sin\psi/\sigma) - (\zeta/l^2) - B$ and ψ varies from 0 at the origin to θ (the contact angle) at the contact line. The boundary conditions are

$$\zeta(0) = 0 \quad \text{and} \quad \sigma(0) = 0 \tag{A4}$$

and the drop volume constraint is

$$\pi \int_{-d}^{0} \sigma^2 d\zeta = V_D \tag{A5}$$

with d as the maximum drop height in the z direction.

Equations (A2) and (A3) are solved with the boundary conditions [Eq. (A4)] using a fourth-order Runge–Kutta (RK4) method. Because the value of B is unknown to start with, the Newton–Raphson method is iteratively used with the volume constraint [Eq. (A5)] to get the correct value of parameter B.

APPENDIX 2: THREE-DIMENSIONAL YOUNG–LAPLACE EQUATION

The Young–Laplace equation for a 3D drop is given as (Pozrikidis, 2009)

$$2\kappa_m = \frac{\Delta\rho}{\gamma}\mathbf{g}\cdot\mathbf{z} + B \tag{B1}$$

Here, κ_m is the mean curvature of the liquid–air interface; $\Delta\rho = \rho_{\text{liq}} - \rho_{\text{air}}$; γ is the surface tension of the liquid; $B = \Delta p/\gamma$, where Δp is the excess pressure in the liquid contained within the drop. For a 3D drop surface $z = f(x, y)$, the curvature of the drop is given by

$$\kappa_m = \frac{1}{2}\frac{\left(1+f_x^2\right) f_{yy} - 2f_x f_y f_{xy} + \left(1+f_y^2\right) f_{xx}}{\left(1+f_x^2+f_y^2\right)^{3/2}} \tag{B2}$$

Here, x and y are the coordinates in the plane z = 0 of the three-phase drop contact line as shown in Fig. 2(b). Substituting Eq. (B2) into Eq. (B1) gives the governing equation for the shape of a non-symmetric drop in terms of the function $f(x, y)$. The governing equation is solved subject to the following boundary conditions:

$$f\left(S\right) = 0, \quad \text{where} \quad S\left(x, y\right) = 0 \text{ is the contact line of the drop} \tag{B3}$$

$$\nabla f \cdot \hat{n} = |\nabla f| \sin\theta \quad \text{on} \quad S\left(x, y\right) = 0 \tag{B4}$$

Here, $\hat{n}$ is a normal to the plane z = 0, and θ is the contact angle and a function of the azimuthal angle ϕ [Fig. 2(b)]. Since the excess pressure $\Delta p (= B \times \gamma)$ is an unknown, the governing equation is solved with a drop volume constraint

$$\int f\left(x, y\right) dxdy = V_D, \quad \text{given} \tag{B5}$$

Solving Eq. (B1) with boundary conditions (B3) and (B4) and constraint (B5) is a challenging problem. An alternative approach based on the variational principle has been used in the present study. It is implemented algorithmically using the open-source software, *Surface Evolver* (Brakke, 1992).